PCCP

PAPER

View Article Online
View Journal | View Issue

Cite this: *Phys. Chem. Chem. Phys.*, 2016, **18**, 23872

Revisiting $AgCrSe_2$ as a promising thermoelectric material

Di Wu,*[a] Sizhao Huang,[a] Dan Feng,[a] Bing Li,[b] Yuexing Chen,[a] Jian Zhang[ac] and Jiaqing He*[a]

Received 10th July 2016,
Accepted 4th August 2016

DOI: 10.1039/c6cp04791b

www.rsc.org/pccp

We revisited and investigated a layer-structured thermoelectric material $AgCrSe_2$, which has an extremely low thermal conductivity. After using both differential scanning calorimetry and a comparative laser flash method, we realized that the specific heat of this material, the main contributor to the reported low thermal conductivity, is unlikely to be way below the Dulong–Petit limit as revealed in the literature. Besides, our *in situ* X-ray diffraction pattern up to 873 K indicated the instability of $AgCrSe_2$ over 723 K, where it begins to decompose into Cr_2Se_3 and Ag_2Se. This unexpected decomposition phenomenon resulted in the gradual increment of specific heat and thermal diffusivity, hence the deterioration of the overall thermoelectric performance. We deliberately introduced Ag and Cr vacancies into the lattice for carrier concentration optimization and could achieve an optimal figure of merit of $ZT \sim 0.5$ at 723 K in the nominal composition $Ag_{0.96}CrSe_2$ in the direction perpendicular to the sintering press. Our findings suggest that more thorough investigations are necessary to ensure that $AgCrSe_2$ is a promising thermoelectric material.

I. Introduction

Thermoelectrics, which can facilitate direct energy conversion between electricity and heat, are deemed to be a promising technique to alleviate the increasing energy crisis nowadays. The performance of a thermoelectric material is evaluated by a dimensionless figure of merit: $ZT = (S^2\sigma/\kappa)T$, where S is the Seebeck coefficient, σ is the electrical conductivity, κ is the thermal conductivity and T is the working temperature. The main strategies of increasing the figure of merit ZT can be concluded as power factor ($S^2\sigma$) enhancement and thermal conductivity reduction. The former could be achieved *via* carrier concentration optimization,[1,2] band structure tailoring,[3–6] modulation doping[7–9] *etc.*, while the latter is usually realizable by nano-structuring[10,11] and/or constructing all-scale hierarchical architectures.[12–14] Meanwhile, thermoelectric systems with intrinsically low thermal conductivities, *e.g.*, superionic $Cu_{2-x}Oh$ (Oh = Te,[15] Se[16] and S[17]), partially filled skutterudites,[18] clathrates with caged frameworks,[19] Zintl phases with both covalent and ionic bonds,[20] layer-structured metal oxides[21,22] and materials with unbonded lone-pair valence electrons,[23,24] can provide another choice of achieving extraordinary ZT values.

$AgCrSe_2$ was recognized as a superionic conductor by Murphy[25] *et al.* in the late 1980s, and its room temperature ionic conductivity is moderately high ($\sim 3 \times 10^{-4}$ S cm^{-1}). The superionic conduction in $AgCrSe_2$ originates from the highly mobile Ag^+ ions in 2D layers which are sandwiched by $CrSe_2$ slabs along the *c*-direction. The $CrSe_2$ slabs form a slightly puckered honeycomb lattice, and leave two different tetrahedral sites, just as in the case of $CuCrSe_2$[26] and $CuCrS_2$.[27,28] $AgCrSe_2$ was reported to experience an order–disorder phase transition[29] as temperature increases to around 475 K, where Ag atoms were believed to start a gradual migration from the "ordered" tetrahedral sites to the "disordered" ones. $AgCrSe_2$ was believed to be a promising thermoelectric material largely due to its intrinsically low thermal conductivity,[30] which originates from its layered structure and "liquid"-like specific heat as seen in the more famous superionic thermoelectric material $Cu_{2-x}Se$.[16] Recently, a low temperature inelastic neutron scattering experiment together with a thermal transport evolution with magnetic field further indicated that the intrinsically low thermal conductivity observed in $AgCrSe_2$ could be attributed to acoustic phonon scattering by a regular lattice of Ag^+ oscillating in quasi-2D potential wells.[31]

Considering the already low thermal conductivity of $AgCrSe_2$, in this specific work, we introduced Ag and Cr vacancies separately into the lattice, seeking for an optimized carrier concentration. We observed anisotropic charge carrier transport in this

[a] *Shenzhen Key Laboratory of Thermoelectric Materials, Department of Physics, South University of Science, Technology of China, Shenzhen 518055, China. E-mail: wud@sustc.edu.cn, he.jq@sustc.edu.cn*
[b] *Japan Proton Accelerator Research Complex, Japan Atomic Energy Agency, Tokai, Ibaraki 319-1195, Japan*
[c] *Key Laboratory of Materials Physics, Institute of Solid State Physics, Chinese Academy of Science, Hefei 230032, China*

material which was not revealed in the previous work,[30,32] and found the electrical conductivity could be enhanced significantly as the number of Ag vacancies increased. More interestingly, we realized that the specific heat of this material, the main contributor to the reported low thermal conductivity, is unlikely to be way below the Dulong–Petit limit as reported.[30] Besides, the *in situ* X-ray diffraction patterns up to 873 K further indicated that $AgCrSe_2$ is not thermally stable over 723 K, where it begins to decompose into Cr_2Se_3 and Ag_2Se. This unexpected decomposition phenomenon resulted in the gradual increment of specific heat and thermal diffusivity, hence a dramatic increase of the thermal conductivity. Eventually, we obtained an optimal figure of merit of $ZT \sim 0.5$ at 723 K in the nominal composition $Ag_{0.96}CrSe_2$ in the direction perpendicular to the sintering press. Although a higher ZT value $\sim$0.54 was observed at 773 K in $Ag_{0.96}CrSe_2$, it is more like a combined effect of microstructure change, phase separation and carrier concentration tuning. Our findings indicate that more thorough investigations are necessary to assure $AgCrSe_2$ a promising thermoelectric material.

II. Sample synthesis and characterization

First, powdery elements of Ag (99.99%, Alfa Aesar), Cr (99.9%, Alfa Aesar) and Se (99.999, Alfa Aesar) were hand-milled with agate mortar and pestle for 10 min to achieve homogeneity. The obtained mixture was cold-pressed under 300 MPa uniaxial pressure into a pellet, which was then evacuated ($<5 \times 10^{-4}$ Pa) and sealed in a quartz tube. The solid state reaction recipe is as follows: the container was heated up to 200 °C in 4 hours, retained at that temperature for another 4 hours, then slowly heated up to 900 °C in 12 hours, and kept at that temperature for another 2 days. After furnace-cooled to room temperature, the obtained compounds were taken out from the quartz and hand-milled into powders for follow-up spark plasma sintering (SPS, Dr Sinter, Japan). The sintering process took place at 700 °C for 5 min under the uniaxial pressure of 50 MPa; the obtained pellets were then cut into rectangular pieces of $\sim 12 \times 2 \times 2$ mm for electrical transport measurements, while coins of $\Phi \sim 10$ mm and thickness of 2 mm were used for thermal diffusivity measurements.

Seebeck coefficient S and electrical resistivity ρ were measured simultaneously in a commercial ZEM-3 (Ultravac, Japan) under an atmosphere of argon; the uncertainty of the measurements is estimated to be within $\sim$5% for each parameter. Thermal diffusivity D was measured in a state-of-art LFA 457 (Netzsch, Germany). For the specific heat C_p, we conducted the measurement using two different methods: one is a comparative method using pyroceram as the reference sample in a LFA 457, and the other is a differential scanning calorimetry (DSC) method using STA 449 (Netzsch, Germany). The different results regarding the two methods will be discussed in the follow-up section. Mass densities ρ of the samples were derived using the state-of-art Archimedes method. Thermal conductivity was calculated using $\kappa = D\, C_p\, \rho$.

Powder X-ray diffraction (XRD) patterns were taken using a Smartlab (9 kW, Rigaku, Japan) equipment and the *in situ* XRD measurement was conducted under vacuum. Scanning electron microscopy (SEM) images were taken using a Zeiss Merlin microscope. Carrier concentrations and mobility were measured in a Lakeshore 8400 Hall measurement station using the van der Pauw method; the samples were polished to be thinner than 1 mm for the measurements.

III. Results and discussions

The powder X-ray diffraction patterns of $Ag_{1-x}CrSe_2$ powders before SPS processes were compared with the standard PDF card and found to be fully consistent with the *R*3*m* type $AgCrSe_2$ (PDF#24-0872) with the layered structure, Fig. 1. As Ag vacancies increased, the single $AgCrSe_2$ phase was retained until x exceeded 0.10. Characteristic peaks of Cr_2Se_3 (PDF#40-1404) and Se (PDF#06-0362) were noticed in the nominal composition $Ag_{0.8}CrSe_2$, implying a partial collapse of the layered *R*3*m* lattice of $AgCrSe_2$. We also examined the $AgCrSe_2$ sample which experienced a heating cycle of thermal diffusivity measurements (up to 550 °C), and found the *R*3*m* structure remained.

The cross-section scanning of the fractured $AgCrSe_2$ sample *via* SEM, shown in Fig. 2(d) and (e), exhibits a lamellar grain structure. Smaller particles in the range of $<$100 nm were also seen at the grain boundaries. The lamellar feature of $AgCrSe_2$ grains suggests a possibly higher charge carrier conduction in the in-plane direction than the off-plane direction. Indeed, measurements of $AgCrSe_2$ exhibited a more than 2-fold difference in electrical conductivity between the parallel and perpendicular directions, despite that imparities in Seebeck coefficients and thermal diffusivities were nearly unnoticeable, Fig. 2(a)–(c). Similar lamellar microstructures were observed before,[30,32] yet no obvious anisotropy was disclosed probably due to the different sintering methods, *i.e.*, SPS in this case and HP in their cases. Considering the obvious superior thermoelectric performance in the perpendicular direction, hereafter,

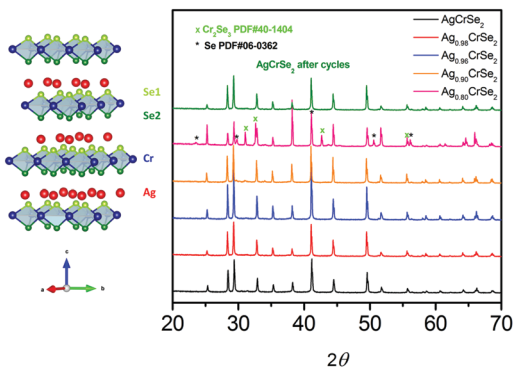

Fig. 1 $AgCrSe_2$ crystal structure with $CrSe_2$ layers and Ag layers stacking alternatively along the *c*-axis. XRD patterns showing all of the $Ag_{1-x}CrSe_2$ (x = 0, 0.02, 0.04, and 0.10) samples crystalize into a *R*3*m* (PDF#24-0872) type structure; however, the Cr_2Se_3 and Se characteristic peaks emerge when x increases to 0.20. The *R*3*m* structure was maintained even after one thermal diffusivity measurement cycle.

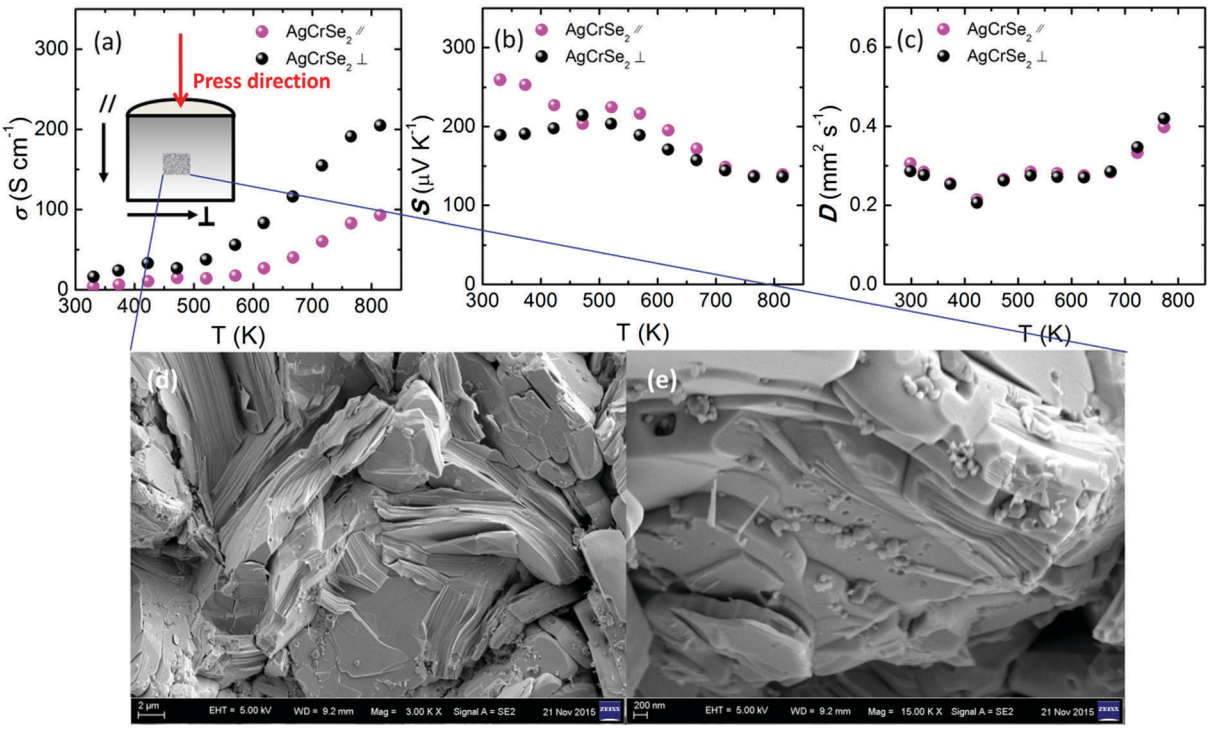

Fig. 2 (a) Electrical conductivity, (b) Seebeck coefficient and (c) thermal diffusivity of $AgCrSe_2$ measured parallel and perpendicular to the press direction showing strong anisotropic features; (d and e) SEM images of the cross-section of $AgCrSe_2$ sample indicating the feature of layered plates when combined with nanoscale particles.

our characterizations and discussions will be restricted to this direction only.

The electrical conductivity for pristine $AgCrSe_2$ is not promising at all to assure it as a decent thermoelectric material, Fig. 3(a). As suggested by Hall measurements (Table 1), pristine $AgCrSe_2$ exhibits the p-type conduction, and the room temperature hole concentration is only $\sim 3.5 \times 10^{18}$ cm^{-3}. This leaves a broad space for carrier concentration optimization. We hereby deliberately introduced Ag vacancies as p-type doping, and lifted up the hole concentration to about 1.46×10^{20} cm^{-3} in $Ag_{1-x}CrSe_2$ as $x = 0.10$. Meanwhile, the carrier mobility only decreased from 21.3 to 14.5 mm^2 (V s)$^{-1}$. Accordingly, at 323 K, the electrical conductivity increased from 13.5 S cm^{-1} to 432.2 S cm^{-1}, and the power factor increased from 0.92 to 2.55 μW (cm K^2)$^{-1}$, as x varied from 0 to 0.10. Pristine $AgCrSe_2$ exhibits a non-degenerate semiconducting behavior as seen from its increasing electrical conductivity σ with temperature. As the hole concentration increases, in $Ag_{0.98}CrSe_2$, the electrical conductivity begins to behave more like a degenerate semiconductor. Indeed, in $Ag_{0.90}CrSe_2$, σ decreases all the way from 432.2 at 323 K to 160.9 S cm^{-1} at 823 K. Note that we deliberately skipped the data points around the phase transition temperature in order to avoid any misleading information. It was very interesting to see that the electrical conductivities and Seebeck coefficients of different samples tended to converge as temperature surpassed 723 K, resulting in approximately the same power factor at high temperatures. In contrast, S and σ were very different at 323 K when x varied. This convergence of electrical properties might originate from the decomposition of $AgCrSe_2$, evidence of which will be discussed in detail in a later section.

Thermal diffusivities of $Ag_{1-x}CrSe_2$ (x = 0, 0.02, 0.04 and 0.10) were measured using a laser flash method, Fig. 4(a). A gradual phase transition, which is indicated by the dip in thermal conductivity values, was observed in all $Ag_{1-x}CrSe_2$ samples. The observed finishing temperature of this phase transition was around 473 K, which agrees very well with the reported order–disorder phase transition point at 475 K.[30] The room temperature diffusivity values of $Ag_{1-x}CrSe_2$ are very low, ranging from 0.268 mm^2 s^{-1} in pristine $AgCrSe_2$ to 0.359 mm^2 s^{-1} in $Ag_{0.90}CrSe_2$, which is in strong contrast with >1.0 mm^2 s^{-1} in the state-of-art thermoelectric system PbQ (Q = Te, Se, and S). The thermal diffusivity curves remain almost constant when the order–disorder phase transition completes. It is also remarkable that all thermal diffusivity curves were found to be increased when temperature climbs over 723 K, which coincides with the convergence temperature of electrical properties.

Provided the existing controversy about the specific heat C_p of $AgCrSe_2$ in the literature,[30,32] we decided to make a reinvestigation into this problem. The temperature dependent C_p curves measured using the DSC method and the laser flash comparative method showed similar features, as illustrated in Fig. 4(b), where the Dulong–Petit limit is plotted for comparison. Both curves implied a phase transition at around 473 K and a gradual exothermal process above $\sim$700 K; no dramatic C_p reduction was seen in contrast to a previous report.[30] The relatively

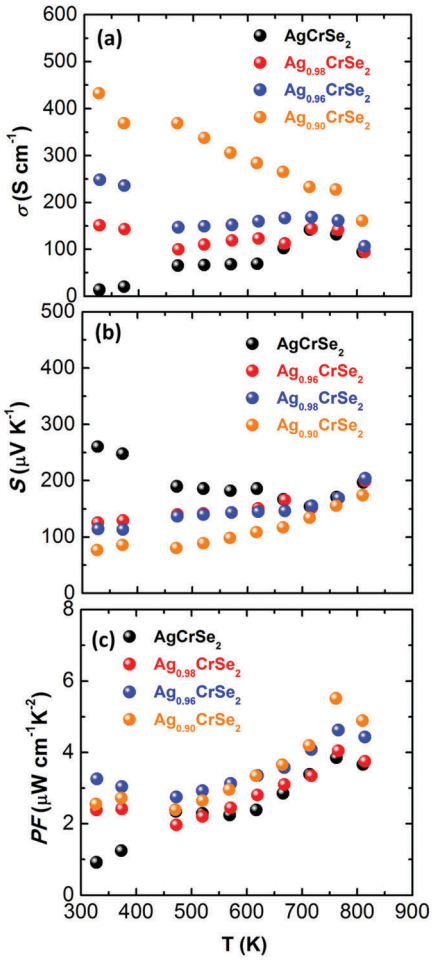

Fig. 3 (a) Electrical conductivity, (b) Seebeck coefficients and (c) power factor of $Ag_{1-x}CrSe_2$ (x = 0, 0.02, 0.04, and 0.10) samples measured from 323 to 823 K.

Table 1 Mass density and derived carrier concentration and mobility at room temperature from Hall measurements

Samples	Mass density (g cm^{-3})	Carrier concentration (cm^{-3})	Carrier mobility (cm^2 V^{-1} s^{-1})
$AgCrSe_2$	6.43 ± 0.09	3.5 ± 0.35 × 10^{18}	21.3 ± 2.1
$Ag_{0.98}CrSe_2$	6.47 ± 0.10	8.0 ± 0.80 × 10^{19}	16.0 ± 1.6
$Ag_{0.96}CrSe_2$	6.43 ± 0.09	8.5 ± 0.85 × 10^{19}	13.5 ± 1.4
$Ag_{0.90}CrSe_2$	6.40 ± 0.09	1.46 ± 0.15×10^{20}	14.5 ± 1.5

constant C_p values between 470 and 700 K (in the highly mobile disorder phase) suggest that the liquid-like superionic conduction in $AgCrSe_2$ is comparatively weak, unlike the superionic $Cu_{2-x}Se$ where C_p gradually decreases with temperature owing to the hopping of Cu^+ ions.[16] Our finding is consistent with Murphy *et al.*,[25] who reported the room temperature superionic conductivity of pristine $AgCrSe_2$ was only ~3 × 10^{-4} S cm^{-1}. The astonishingly low C_p reported before[30] might merely be an artificial result of the endothermal process due to oxidization during the DSC measuring cycle.

To avoid any further inconsistency, we utilize the Dulong–Petit limit of specific heat (~0.31 J g^{-1} K^{-1}) to calculate the

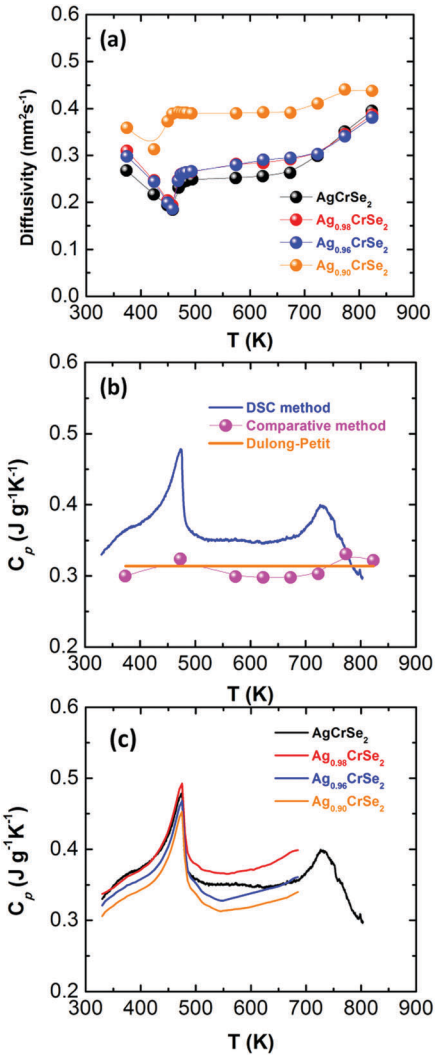

Fig. 4 (a) Thermal diffusivities of $Ag_{1-x}CrSe_2$ (x = 0, 0.02, 0.04 and 0.10) measured in the range of 323–823 K, indicating the phase transition temperature to be at ~470 K; this was confirmed by specific heat C_p measurements of pristine $AgCrSe_2$ (b) using both the comparative method and the DSC method. The Dulong–Petit limit is plotted here as a comparison. The gradual increment of C_p after ~700 K might originate from the decomposition of $AgCrSe_2$ at high temperature. (c) Comparison of C_p values of $Ag_{1-x}CrSe_2$ (x = 0, 0.02, 0.04 and 0.10) measured using the DSC method.

thermal conductivity, and the result is shown in Fig. 5(a). The thermal conductivity values were found to be decreased at the beginning then levelled out after the order–disorder phase transition at around 470 K. As temperature climbs higher up to 723 K, the thermal conductivity increases significantly. The electronic contribution to the thermal conductivity is calculated using the Wiedemann–Franz relation $\kappa_e = L\sigma T$, where Lorenz number L can be estimated by fitting experimental Seebeck values in a single parabolic band model.[33] Lattice thermal conductivity κ_L, shown in Fig. 5(d), is derived by subtracting the electronic part from the total thermal conductivity. The bipolar contribution is not considered here because the intrinsic activation of electrons from valence bands to conduction bands is unlikely to happen in $AgCrSe_2$ considering the reported wide

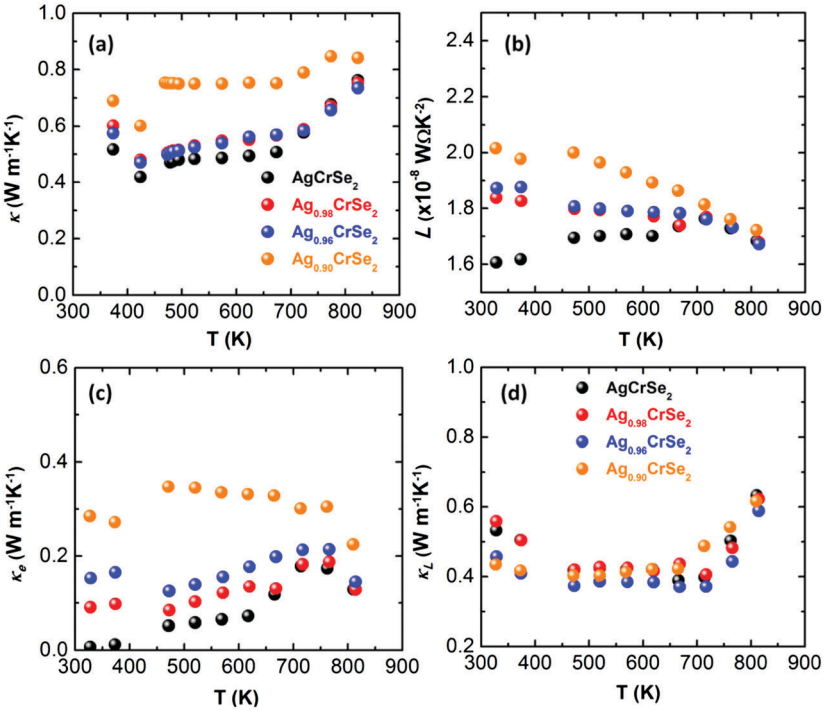

Fig. 5 (a) Total thermal conductivity, (b) Lorenz number, (c) electronic thermal conductivity and (d) lattice thermal conductivity of $Ag_{1-x}CrSe_2$ (x = 0, 0.02, 0.04 and 0.10) samples measured from 323 to 823 K.

band gap of $AgCrSe_2$ ~0.49 eV[32] at room temperature. The calculated lattice thermal conductivity values are not too much different from each other despite the composition variation from $AgCrSe_2$ to $Ag_{0.90}CrSe_2$, indicating that the scattering effect of Ag vacancies on heat-carrying phonons is very limited. This suggests that the ultralow thermal conductivity in $AgCrSe_2$ is intrinsic, which agrees with the proposal by Damay *et al.* that acoustic phonon scattering is dominated by a regular lattice of Ag^+ oscillating in quasi-2D potential wells.[31]

Combined with the power factors calculated earlier, the intrinsically low thermal conductivities produced a moderate figure of merit ZT in $Ag_{1-x}CrSe_2$ (x = 0, 0.02, 0.04 and 0.10) samples, Fig. 6. The maximal value of ZT ~ 0.55 was found in $Ag_{0.96}CrSe_2$ at 773 K. This value is only ~25% higher than that of pristine $AgCrSe_2$ at the same temperature, owing to the unexpected convergence of power factors and the dramatic increase of thermal conductivity values; nevertheless, ZT at 323 K was increased from 0.048 of pristine $AgCrSe_2$ to 0.157 of $Ag_{0.96}CrSe_2$, a ~225% enhancement resulting from the carrier concentration optimization.

To find out the underlying mechanism of the unexpected power factor convergence and thermal conductivity increase at around 723 K, we conducted an *in situ* XRD measurement in a heating cycle from 323 to 873 K for pristine $AgCrSe_2$, Fig. 7. No obvious peak shifts could be found in these typical characteristic peaks of $AgCrSe_2$, *e.g.*, (1 0 1), (0 1 2), (1 0 4), (0 0 9) (1 0 7), and (0 1 8) planes. However, we did notice the disappearance or weakening of the (1 0 5) peak as the temperature went over 473 K. This might be related to the Ag^+ ion migration from the "ordered" tetragonal sites to the "disordered" ones during the order–disorder phase transition. As temperature kept on

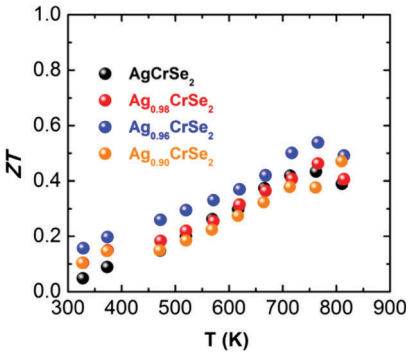

Fig. 6 Figure of merit ZT of $Ag_{1-x}CrSe_2$ (x = 0, 0.02, 0.04 and 0.10) samples. A maximal ZT of 0.55 was achieved in $Ag_{0.96}CrSe_2$ at 773 K.

increasing, the characteristic peaks of the Cr_2Se_3 $P\bar{3}m1$ phase, *e.g.*, (0 0 2), (1 0 1), and (1 0 2), started to emerge. This suggests a possible decomposition of $AgCrSe_2$ into Cr_2Se_3 and Ag_2Se. The turning point was at around 723 K, exactly the same temperature where power factor started to converge and thermal conductivity began to increase. Therefore, we are encouraged to ascribe the unexpected powder factor convergence and thermal conductivity increase to the partial decomposition of $AgCrSe_2$ without further investigation. We need to emphasize that the crystallographic $R3m$ structure of the $AgCrSe_2$ sample still remained after experiencing a heating cycle of thermal diffusivity measurement (up to 550 °C), as shown in Fig. 1. This information is important since it not only implies the decomposition process is reversible, but also gives $AgCrSe_2$ credit as a candidate thermoelectric material at least below 723 K.

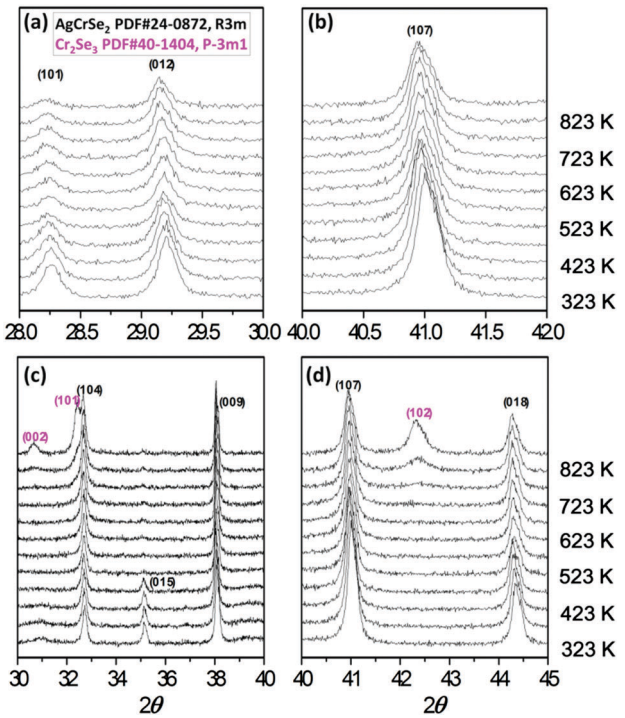

Fig. 7 The *in situ* XRD patterns of $AgCrSe_2$ in a heating process from 323 to 873 K. (a and b) No obvious shifts were found for the $AgCrSe_2$ characteristic peaks, except that (c) the (0 1 5) peak disappeared or was weakened over 473 K, probably indicating the change of Ag occupation from the disordered to the ordered one. (d) When temperature went up over 723 K, characteristic peaks of Cr_2Se_3 show up as a result of $AgCrSe_2$ decomposition.

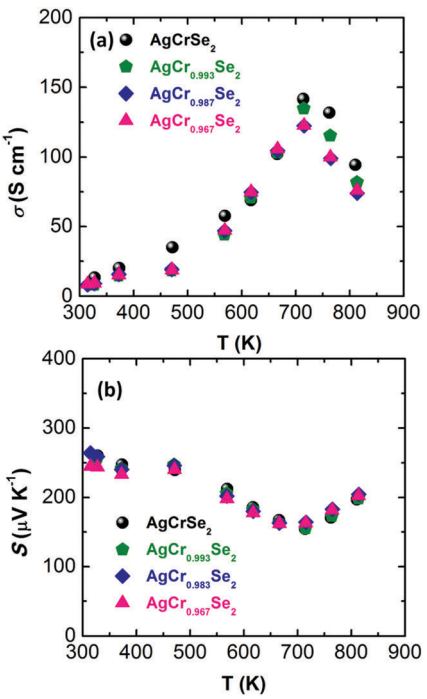

Fig. 8 (a) Electrical conductivity and (b) Seebeck coefficient of $AgCr_{1-y}Se_2$ (y = 0.007, 0.013 and 0.033) samples measured from 323 to 823 K.

Trials of introducing Cr vacancies into $AgCrSe_2$ were also performed; the number of Cr vacancies was deliberately selected in order to theoretically provide the same hole density to the $AgCrSe_2$ lattice as what Ag vacancies did in our above work. Unfortunately, no noticeable effect on electrical transport properties could be traced (Fig. 8). The reason might lie in the inefficient charge transfer between the conducting Ag^+ layers and the insulating $CrSe^{2-}$ framework, as the electronic band structure of $CuCrSe_2$ *via* density functional calculation suggested.[34]

IV. Conclusions

We reinvestigated the superionic thermoelectric $AgCrSe_2$, and found that Ag vacancies rather than Cr vacancies are effective p-type dopants. The maximal figure of merit $ZT \sim 0.5$ was achieved in the nominal composition $Ag_{0.96}CrSe_2$ at 723 K in the direction perpendicular to the imposed sintering press. Further increment of ZT up to 0.55 in the same sample might originate from a mixed effect of microstructure evolution, phase separation and carrier concentration optimization. Through differential scanning calorimetry and laser flash comparative methods, we realized the specific heat of $AgCrSe_2$ is dissimilar to the reported liquid-like behaviors. Moreover, we found the decomposition phenomenon of $AgCrSe_2$ when temperature climbed above 723 K; this was believed to be responsible for the observed convergence of electrical properties and the increase of thermal conductivity. Our findings suggest that a more thorough investigation into $AgCrSe_2$ is necessary to ensure $AgCrSe_2$ is a promising thermoelectric material.

Acknowledgements

This contribution was supported by the startup of South University of Science and Technology of China (JQH), NSFC under Grant No. 11504160 (DW), National 1000 Plan for Young Scientists (JQH), and also partially supported by the Science, Technology and Innovation Commission of Shenzhen Municipality (Grant No. JCYJ 20140612140151884 and KQCX2015033110182370).

References

1 Y. Pei, A. F. May and G. J. Snyder, *Adv. Energy Mater.*, 2011, **1**, 291–296.
2 L.-D. Zhao, G. Tan, S. Hao, J. He, Y. Pei, H. Chi, H. Wang, S. Gong, H. Xu and V. P. Dravid, *Science*, 2016, **351**, 141–144.
3 J. P. Heremans, V. Jovovic, E. S. Toberer, A. Saramat, K. Kurosaki, A. Charoenphakdee, S. Yamanaka and G. J. Snyder, *Science*, 2008, **321**, 554–557.
4 Y. Pei, X. Shi, A. LaLonde, H. Wang, L. Chen and G. J. Snyder, *Nature*, 2011, **473**, 66–69.
5 D. Wu, L. D. Zhao, S. Hao, Q. Jiang, F. Zheng, J. W. Doak, H. Wu, H. Chi, Y. Gelbstein, C. Uher, C. Wolverton, M. Kanatzidis and J. He, *J. Am. Chem. Soc.*, 2014, **136**, 11412–11419.

6 G. Tan, F. Shi, S. Hao, H. Chi, T. P. Bailey, L.-D. Zhao, C. Uher, C. Wolverton, V. P. Dravid and M. G. Kanatzidis, *J. Am. Chem. Soc.*, 2015, **137**, 11507–11516.
7 D. Wu, Y. Pei, Z. Wang, H. Wu, L. Huang, L.-D. Zhao and J. He, *Adv. Funct. Mater.*, 2014, **24**, 7763–7771.
8 M. Zebarjadi, K. Esfarjani, Z. Bian and A. Shakouri, *Nano Lett.*, 2011, **11**, 225–230.
9 Y. L. Pei, H. Wu, D. Wu, F. Zheng and J. He, *J. Am. Chem. Soc.*, 2014, **136**, 13902–13908.
10 N. Mingo, D. Hauser, N. Kobayashi, M. Plissonnier and A. Shakouri, *Nano Lett.*, 2009, **9**, 711–715.
11 B. Poudel, Q. Hao, Y. Ma, Y. Lan, A. Minnich, B. Yu, X. Yan, D. Wang, A. Muto and D. Vashaee, *Science*, 2008, **320**, 634–638.
12 H. J. Wu, L. D. Zhao, F. S. Zheng, D. Wu, Y. L. Pei, X. Tong, M. G. Kanatzidis and J. Q. He, *Nat. Commun.*, 2014, **5**, 4515.
13 D. Wu, L.-D. Zhao, X. Tong, W. Li, L. Wu, Q. Tan, Y. Pei, L. Huang, J.-F. Li, Y. Zhu, M. G. Kanatzidis and J. He, *Energy Environ. Sci.*, 2015, **8**, 2056.
14 K. Biswas, J. He, I. D. Blum, C. I. Wu, T. P. Hogan, D. N. Seidman, V. P. Dravid and M. G. Kanatzidis, *Nature*, 2012, **489**, 414–418.
15 Y. He, T. Zhang, X. Shi, S.-H. Wei and L. Chen, *NPG Asia Mater.*, 2015, **7**, e210.
16 H. Liu, X. Shi, F. Xu, L. Zhang, W. Zhang, L. Chen, Q. Li, C. Uher, T. Day and G. J. Snyder, *Nat. Mater.*, 2012, **11**, 422–425.
17 Y.-H. Ji, Z.-H. Ge, Z. Li and J. Feng, *J. Alloys Compd.*, 2016, **680**, 273–277.
18 B. Sales, D. Mandrus and R. K. Williams, *Science*, 1996, **272**, 1325–1328.
19 G. S. Nolas, J. Poon and M. Kanatzidis, *MRS Bull.*, 2006, **31**, 199–205.
20 S. M. Kauzlarich, S. R. Brown and G. J. Snyder, *Dalton Trans.*, 2007, 2099–2107.
21 Y. Wang, N. S. Rogado, R. Cava and N. Ong, *Nature*, 2003, **423**, 425–428.
22 L. D. Zhao, V. P. Dravid and M. G. Kanatzidis, *Energy Environ. Sci.*, 2014, **7**, 251.
23 D. Morelli, V. Jovovic and J. Heremans, *Phys. Rev. Lett.*, 2008, **101**, 035901.
24 A. Walsh, D. J. Payne, R. G. Egdell and G. W. Watson, *Chem. Soc. Rev.*, 2011, **40**, 4455–4463.
25 D. Murphy, H. Chen and B. Tell, *J. Electrochem. Soc.*, 1977, **124**, 1268–1271.
26 G. C. Tewari, T. S. Tripathi, H. Yamauchi and M. Karppinen, *Mater. Chem. Phys.*, 2014, **145**, 156–161.
27 Y.-X. Chen, B.-P. Zhang, Z.-H. Ge and P.-P. Shang, *J. Solid State Chem.*, 2012, **186**, 109–115.
28 G. C. Tewari, T. Tripathi, P. Kumar, A. Rastogi, S. Pasha and G. Gupta, *J. Electron. Mater.*, 2011, **40**, 2368–2373.
29 A. Van Der Lee and G. Wiegers, *J. Solid State Chem.*, 1989, **82**, 216–224.
30 F. Gascoin and A. Maignan, *Chem. Mater.*, 2011, **23**, 2510–2513.
31 F. Damay, S. Petit, S. Rols, M. Braendlein, R. Daou, E. Elkaim, F. Fauth, F. Gascoin, C. Martin and A. Maignan, *Sci. Rep.*, 2016, **6**, 23415.
32 S. Bhattacharya, A. Bohra, R. Basu, R. Bhatt, S. Ahmad, K. N. Meshram, A. K. Debnath, A. Singh, S. K. Sarkar, M. Navneethan, Y. Hayakawa, D. K. Aswal and S. K. Gupta, *J. Mater. Chem. A*, 2014, **2**, 17122–17129.
33 D. Wu, L. D. Zhao, F. Zheng, L. Jin, M. G. Kanatzidis and J. He, *Adv. Mater.*, 2016, **28**, 2737–2743.
34 D. Srivastava, G. C. Tewari, M. Karppinen and R. Nieminen, *J. Phys.: Condens. Matter*, 2013, **25**, 105504.

